Available online at www.sciencedirect.com
ScienceDirect
Earth and Planetary Science Letters 261 (2007) 217–229
EPSL
www.elsevier.com/locate/epsl

The effect of oxygen fugacity on hydroxyl concentrations and speciation in olivine: Implications for water solubility in the upper mantle

K.J. Grant [a,b,*], R.A. Brooker [a,c], S.C. Kohn [a], B.J. Wood [b]

[a] Department of Earth Sciences, University of Bristol, Wills Memorial Building, Queens Road, Bristol, BS8 1RJ, UK
[b] ARC Key Centre for the Geochemistry and Metallogeny of the Continents (GEMOC), Department of Earth and Planetary Sciences, Macquarie University, NSW, Australia
[c] Department of Earth Sciences, University College London, Gower Street, London. WC1E 6BT, UK

Received 5 February 2007; received in revised form 20 June 2007; accepted 22 June 2007
Available online 3 July 2007
Editor: R.W. Carlson

Abstract

The effect of oxygen fugacity on hydroxyl speciation and solubility in San Carlos olivine was investigated in a series of piston cylinder experiments at 2.0 GPa and 1100 and 1300 °C. The presence of enstatite was intended to fix silica activity and experimental fO_2 in most runs was regulated by lining the inner walls of the sample-containing Pt capsules with either Fe, Ni or Re foil. Polarised infrared absorbance spectra show that olivine annealed in capsules lined with Fe foil only contain hydroxyl defects with vibrational energies between 3650 and 3400 cm^{-1} (relatively high frequencies). Spectra of crystals annealed in capsules lined with Ni or Re foil show that these samples contain hydroxyl defects with vibrational energies between 3650 and 3400 cm^{-1} (high frequency), and at 3355 and 3325 cm^{-1} (low-frequency). The concentrations of hydroxyl defects responsible for absorptions at 3355 and 3325 cm^{-1} change as a function of oxygen fugacity and are, therefore, interpreted as Fe^{3+}-related OH centres.

Hydroxyl solubility in our experiments is substantially less than current solubility laws might suggest. These differences may be attributed to variations in experimental procedure, but they also demonstrate that the incorporation of hydroxyl in olivine must be better understood before an accurate model to describe water solubility in the deep Earth can be constructed. Our data show that, when experiments conducted at identical P–T conditions are compared, olivine annealed at low fO_2 (below Fe–FeO) contains less than half as much water as crystals from relatively more oxidised experiments. Because natural mantle conditions approximate to those of our low fO_2 experiments, current solubility laws – which are based on data from relatively high fO_2 experiments – overestimate the amount of water that can be hosted in olivine in the upper mantle. From a consideration of defect equilibria we propose a mechanism for the incorporation of OH in olivine in a way that is appropriate for the actual range of conditions expected in the mantle.

Keywords: oxygen fugacity; water; solubility; olivine; upper mantle

1. Introduction

Olivine is volumetrically the most important mineral of the Earth's upper mantle. Natural, mantle-derived olivines contain up to a maximum of several hundred ppm H_2O, but typically contain 100 ppm or less (Miller et al., 1987; Bell et al., 2004; Matsyuk and Langer, 2004;

* Corresponding author. Tel.: +61 29850 8258; fax: +61 29850 8943.
E-mail addresses: kgrant@els.mq.edu.au (K.J. Grant), richard.brooker@ucl.ac.uk (R.A. Brooker), simon.kohn@bristol.ac.uk (S.C. Kohn), bwood@els.mq.edu.au (B.J. Wood).

0012-821X/$ - see front matter © 2007 Elsevier B.V. All rights reserved.
doi:10.1016/j.epsl.2007.06.024

Mosenfelder et al., 2006a; Grant et al., 2007a). At high pressures and temperatures, hydrous synthetic olivine can hold several thousand ppm H_2O (Kohlstedt et al., 1996; Mosenfelder et al., 2006b; Smyth et al., 2006). Experimental studies have demonstrated that hydroxyl defect species in olivine are dominantly associated with point defects in the crystal lattice (Bai and Kohlstedt, 1992; Bai and Kohlstedt, 1993; Kohlstedt et al., 1996; Matveev et al., 2001; Lemaire et al., 2004; Zhao et al., 2004; Berry et al., 2005; Matveev et al., 2005; Smyth et al., 2006; Grant et al., 2006; Mosenfelder et al., 2006b; Berry et al., in press). Kohlstedt et al. (1996) used the results of high-pressure and temperature experiments to suggest that water solubility in olivine increases as a function of fH_2O. These results, and those of a subsequent study (Mosenfelder et al., 2006b), are now used as a framework with which to estimate the maximum amount of water dissolved in olivine at depth in the Earth. Both of these sets of experiments were, however, conducted under relatively oxidising conditions (mostly at, or near to, the Ni–NiO buffer, NNO). Natural, mantle-derived samples indicate that oxygen fugacity in the lithosphere is heterogeneous and that fO_2 decreases systematically through the garnet peridotite field of the upper mantle (Wood and Virgo, 1989; McCammon et al., 2001; Woodland and Koch, 2003). It has been estimated that at depths of greater than 200 km, the intrinsic log fO_2 of unmetasomatised upper mantle may be 4 log units below the QFM buffer (QFM-4)(McCammon et al., 2001; Woodland and Koch, 2003). The effect that the increased fH_2 relative to fH_2O under such reducing conditions has on the solubility of water in olivine remains largely unexplored.

The effect of fO_2 on hydroxyl solubility in olivine is also of great interest because it has been suggested that it may be important for the development of hydroxyl defects with vibrational energies between 3400 and 3200 cm^{-1} (Berry et al., 2005; Mosenfelder et al., 2006b). The precise speciation of these hydroxyl defects has proven extremely controversial (Bai and Kohlstedt, 1993; Matveev et al., 2001, 2005; Lemaire et al., 2004; Berry et al., 2005; Mosenfelder et al., 2006a,b; Smyth et al., 2006; Demouchy and Mackwell, 2006) and is of considerable geological significance because they are commonly, but not ubiquitously, found in natural samples. Recently, for example, Grant et al. (2007a) studied olivines from three different peridotite xenoliths from Kilbourne Hole, New Mexico. Olivines from one xenolith contained only OH absorptions between 3400–3300 cm^{-1}, one only between 3650–3400 cm^{-1} and one contained both groups of species.

With these considerations in mind we devised a series of high-pressure and temperature experiments to isolate the effect of fO_2 on hydroxyl defect speciation and concentrations in mantle olivine. We followed the experimental approach employed by Kohlstedt et al. (1996), with the exceptions that the experiments in our study were conducted at a single pressure (2.0 GPa), at two different temperatures (1100 and 1300 °C) and using a range of oxygen buffers. Throughout this manuscript we use the term "annealed" to describe our experiments aimed at approaching point defect equilibrium between initially anhydrous olivines with a hydrous fluid at a range of imposed oxygen fugacities. High-pressure (and therefore high fH_2O) increases the number of OH-related defects, thus allowing us to make the spectroscopic observations as well as determining the maximum water solubility in the samples under these conditions. The aim of our experiments was to re-equilibrate the point defect population dissolved in San Carlos olivine at the experimentally imposed conditions, not simply to 'decorate' defects already present in the starting crystals.

2. Experimental methods

2.1. Starting crystals

Two different sets of natural olivine single crystals from San Carlos, Arizona were used in this study (Table 1). The first, SC8803B, were small (0.5–2 mm diameter) crystals (approximate composition Fo_{90}) separated from a Type I lherzolite mantle xenolith (Wood and Virgo, 1989). The second were extremely large olivine crystals (approximate composition $Fo_{90.5}$) that were kindly donated by D.L. Kohlstedt (University of Minnesota). Initially measuring several centimetres in diameter, these large crystals were cut into cubes of approximately 2 mm × 2 mm × 2 mm with surfaces parallel to the (001), (010), and (100) crystallographic planes (Fig. 1).

2.2. Analytical procedures

Major element compositions were determined using the Cameca SX100 electron microprobe in the Department of Earth Sciences, Macquarie University using a range of silicate standards and employing an accelerating voltage of a 15 kV and beam current of 20 nA. The concentrations of selected rare earth and other trace elements were measured *in situ* on polished sections of the starting crystals using the laser ablation ICP-MS microprobe at Macquarie University. Details of the experimental setup are provided elsewhere (Grant et al., 2007b).

Polarised infrared absorbance spectra were collected using a NicPlan infrared microscope and Nicolet Nexus FTIR spectrometer. 512 scans, collected in the range 5500

Table 1
Major element and trace element compositions of San Carlos olivine used as starting materials

	Starting olivine	
	SC8803B	SC cube
SiO_2	40.4	40.0
FeO	9.6	9.4
MgO	49.6	50.5
MnO	0.2	0.1
CaO	0.1	0.1
NiO	0.4	0.4
Total	100.3	100.5
n [a]	6	6
Li	1(0.1)	2(0.1)
Be	0.2(0)	b.d.l.
B	4(1)	3(0.4)
Na	42(3)	41(3)
Al	74(11)	94(4)
P	30(15)	26(2)
Ca	413(9)	452(33)
Sc	3(0.1)	3(0.1)
Ti	21(4)	9(0.3)
V	3(0.1)	3 (0.1)
Cr	92 (2)	89(2)
Co	141 (1)	138(1)
Cu	1(0.1)	10(0.4)
Zn	56(1)	50(0.8)
Ga	0.1(0.01)	0.1(0.03)
Sr	0.03(0.02)	0.01(0.01)
Y	0.04(0.03)	0.01(0.01)
Zr	0.05(0.02)	0.02(0.01)
Pb	0.2(0.2)	0.2(0.1)

Trace elements quantified using LA-ICP-MS at Macquarie University.
[a] Number of analyses.

to 650 cm^{-1}, were accumulated to generate each spectrum. A Globar source, KBr beamsplitter and dedicated liquid nitrogen-cooled MCT detector were used to collect spectra with a spectral resolution of 4 cm^{-1}. Polarisation of the electric vector was attained using a ZnSe wire grid polariser located in the microscope. At least ten separate spectra were collected from each sample.

The thickness of each wafer was measured using a Mitutoyo digimatic indicator. Wafers were generally 150–350 μm thick. All raw spectra were normalised to a 1 cm pathlength. Polynomial backgrounds, adjusted individually to obtain a sample-specific best fit, were subtracted from each spectrum. In experiments where olivine single crystals from SC8803B were used, spectra were collected on a number of individual crystals from each sample. Cubes of San Carlos olivine were analysed at numerous positions across the sample slice.

Polarised spectra were collected on crystal wafers that were oriented according to crystallographic axes under an optical microscope. The large crystals of olivine (SC cube) contained planes of inclusions parallel to (010) which, when coupled with large physical dimensions, facilitated crystal orientation. Crystallographic orientation was confirmed spectroscopically using the overtone and combination absorptions between 2400 and 1200 cm^{-1} (Lemaire et al., 2004). Crystal alignment is estimated to be better than ±10°.

Hydroxyl contents in each sample were quantified by summing the contributions of all OH absorptions on averaged spectra collected parallel to each crystallographic direction and by measuring the total OH absorption intensity on the background-subtracted total spectrum ($A^{tot}=A^{E||x}+A^{E||y}+A^{E||z}$). Apart from SC10, which is described in greater detail in a later section, total integrated OH absorbances calculated for each sample using both methods are identical (<10% relative to the mean value). Dissolved hydroxyl contents were estimated from the total integrated OH absorbance using the mineral-specific molar absorption coefficient (Bell et al., 2003) and two separate wavenumber-dependent calibrations (Paterson, 1982; Libowitzky and Rossman, 1997).

2.3. High-pressure experiments

Water solubility in olivine was measured after a series of experiments carried out in an end loaded, 3/4 inch diameter piston cylinder apparatus. Each experiment was performed using a talc-pyrex assembly with a tapered graphite furnace. Details of the pressure calibration and thermocouple arrangement are described elsewhere (McDade et al., 2002).

Samples were contained within sealed 6 mm diameter Pt capsules. For all but one experiment, fO_2 was controlled by lining the capsule interior walls with either Fe (SC1, SC2, SC3), Re (SC5) or Ni foil (SC6, SC8, SC10) (Table 2). At the experimental pressure used in

Table 2
Experimental details

	SC1	SC2	SC3	SC5	SC6	SC8	SC10	SC15b
Olivine [a]	8803	8803	8803	8803	8803	cube	cube	8803
Matrix	Talc: bruc	Talc: bruc	Talc: bruc	Talc: bruc	Talc: bruc	Talc: bruc	Talc: bruc	Talc: bruc
T (°C)	1100	1100	1300	1100	1100	1100	1100	1300
P (GPa)	2	2	2	2	2	2	2	2
fO_2 [b]	Fe	Fe	Fe	Re	Ni	Ni	Ni	None
duration	144 h	4 h	4 h	14 h	14 h	168 h	0.5 h	68 h

[a] Starting olivine: SC8803B = xenolith-derived; cube = large San Carlos crystal.
[b] fO_2 controlled by incorporating foil of relevant metal in the capsule (see text).

this study (2.0 GPa), the calculated log fO_2 for the controlling reaction Fe–FeO is −13.1 (at 1100 °C) and −10.7 (at 1300 °C). Experiments have shown that log fO_2 of the reaction Ni–NiO at 2.0 GPa and 1100 and 1300 °C is −8.3 and −6.1, respectively whereas log fO_2 of the reaction Re–ReO_2 at identical P–T conditions is −6.4 and −4.4 (O'Neill, 1988; O'Neill and Pownceby, 1993). In one experiment (SC15b) no buffer foil was included and the intrinsic fO_2 of the high-pressure talc/Pyrex assembly was imposed. The intrinsic fO_2 of the high-pressure assembly used in this study has not been systematically quantified, but is most likely relatively oxidising (see Brooker et al., 1998, for review).

All experiments where the capsule was lined with Fe foil will henceforth be termed "low fO_2" experiments. The term "higher fO_2 experiments" will be applied to those experiments where the sample capsule remained unbuffered or was lined with Ni or Re foil. In each experiment, olivine crystals were embedded in a finely powdered talc:brucite mixture (Kohlstedt et al., 1996). These matrix materials are synthetic and Fe-free. Decomposition of the talc:brucite buffer material at high pressure and temperature yields olivine + enstatite + H_2O, an assemblage intended to fix silica activity at a relatively high value and one that is similar to that of an orthopyroxene-bearing mantle assemblage (see discussion in Matveev et al., 2001). Each experiment comprised approximately 30 SC8803B olivine crystals or a single San Carlos cube interlayered with the talc–brucite mixture (Fig. 1).

Each experiment was initiated by gently increasing the sample pressure to approximately 0.5 GPa. It was then heated to 500 °C to soften the pyrex sleeve. The sample pressure and temperature were then increased to the required conditions. Switching off power to the furnace terminated each experiment. After gradual decompression, the charge was removed from the assembly and pierced to check for the presence of water. Only samples where free fluid was observed exiting from the pierced Pt capsule are described. In all samples buffered by the reactions Fe–FeO and Ni–NiO that we describe, remnant metal foil from the oxygen buffer material and brightly coloured oxide of the corresponding metal was recovered from the capsule. The presence of metal and oxidised material in the capsule indicates that the fO_2 buffer was not exhausted during the experiment. A single experiment was conducted using Re foil oxygen buffer. Crystalline buffer material recovered from the capsules was not analysed and it was impossible to identify oxidised product of this metal buffer in our experiments. It is therefore possible that experimental fO_2 of this run, although relatively oxidising, was not identical to that of the reaction Re–ReO_2.

3. Results

3.1. Olivine chemistry before the annealing experiments

The chemical compositions of both sets of starting olivine from San Carlos were analysed before we conducted the high-pressure annealing experiments. Grains were checked for core-rim homogeneity using electron microprobe and LA-ICPMS. No chemical zoning was detected in any of the starting crystals. Compositionally, the two sets of starting crystals are almost indistinguishable (Table 1), although the Ti contents of SC8803B (20 ppm) are higher than the olivine cubes (<10 ppm). The concentrations of K(0.6), Ga(0.05), Rb (0.03), Nb(0.02), Ba(0.09), La(0.02), Ce(0.02), Pr(0.02), Nd(0.06), Sm(0.07), Eu(0.02), Gd(0.06), Tb(0.01), Dy (0.06), Er(0.05), Yb(0.07), Lu(0.01), Hf(0.04), Ta(0.01), Th(0.01) and U(0.01) were below detection limit in all crystals examined — numbers in brackets following each element are detection limits, in ppm, calculated from

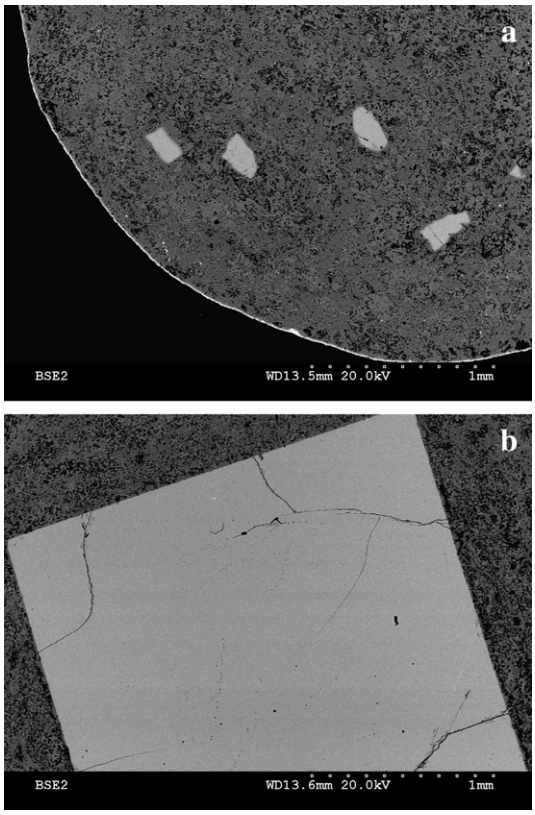

Fig. 1. SEM images of experimental products recovered from experiments a) SC6 and b) SC10. Images show sample capsules before crystals were removed and prepared for infrared analysis. Sections were prepared perpendicular to the capsule length and parallel to the layers of San Carlos starting crystals (in (a)). The lightly coloured rim around sample in (a) is NiO from the metal foil oxygen buffer.

count statistics recorded during analyses of the San Carlos olivines.

Slices of olivine cubes several millimetres thick were analysed (without the microscope) in the spectrometer bench. There was no evidence for any hydroxyl defects in the starting crystals on the resulting unpolarised absorption spectra. The lower limit of water identifiable using this analytical setup is better than that possible using the infrared microscope and is estimated to be less than 0.5 ppm H_2O.

3.2. Olivine after high-pressure experiments

3.2.1. Low fO_2 annealing experiments

SC8803b single crystals were used in all low fO_2 annealing experiments. The major element compositions of olivines recovered from SC1, SC2 and the core of SC3 are identical to the starting crystals (Table 3). An asymmetric iron-rich overgrowth, which is depleted in all other major and trace elements compared to the starting crystals, developed around the starting crystals in SC3. Olivine comprising the rim surrounding olivine in this sample is treated in the following as a separate phase because it is compositionally distinct to the starting crystal (Table 3) and we were able to collect polarised infrared spectra from it (Fig. 2). Fe-rich olivine overgrowths most likely grew from the synthetic talc: brucite (olivine:enstatite at run conditions) matrix in response to an influx of Fe from the buffer foil either transported by the hydrous fluid or migrating through the olivine:enstatite matrix. The physical dimensions of the overgrowths varied, but in places it was 100–200 μm thick. Why asymmetric overgrowths developed is unclear, although it is possible that they were initially

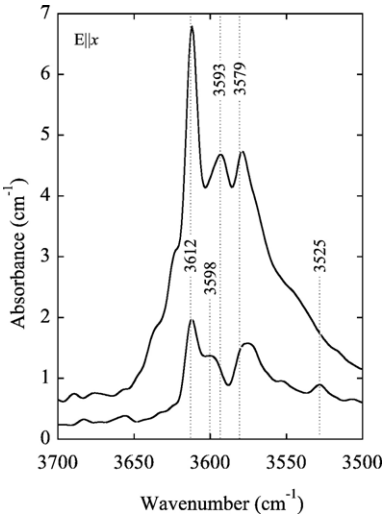

Fig. 2. Spectra showing OH absorptions, measured where $E||x$, collected on samples of re-equilibrated and Fe-rich (lower), re-crystallised olivine (upper spectrum) from SC3. Spectra in all figures have been normalised to a 1 cm pathlength.

of uniform thickness but were fractured during sample preparation.

With the exception of Fe-rich rims and very thin Ni-rich rims on olivine from the Ni-buffered experiments (discussed below), the major element compositions of all phases recovered from the experiments are spatially homogeneous. In contrast to SC3, which was conducted 1300 °C, neither of the lower temperature experiments (SC1 and SC2 were conducted at 1100 °C) developed an Fe-enriched rim around the starting crystals. Thus, our results demonstrate that the growth of secondary olivine is facilitated more by increasing temperature by 200°

Table 3
Major element chemistry and hydroxyl contents of re-equilibrated olivine

	SC1	SC2	SC3		SC5	SC6	SC8	SC10	SC15b
			Core	Rim				Rim	
SiO_2	40.27(0.06)	41.31(0.04)	40.53	39.98	40.95(0.4)	41.06(0.35)	40.26(0.19)	40.04(0.29)	41.76(0.26)
FeO	9.47(0.12)	8.97(0.19)	9.31	13.95	8.66(0.1)	8.64(0.10)	9.35(0.13)	9.36(0.18)	0.96(0.05)
MgO	49.49(0.06)	50.02(0.32)	49.59	46.26	49.85(0.4)	49.94(0.4)	49.71(0.24)	50.47[0.49)	57.13[0.31)
MnO	0.12(0.01)	0.12(0.10)	0.10	0.00	0.12(0.02)	0.12(0.02)	0.12(0.02)	0.13(0.02)	0.01 (0.02)
CaO	0.06(0.00)	0.06(0.00)	0.05	0.010	0.07(0.02)	0.06(0.02)	0.08(0.03)	0.07(0.15)	0.01(0.01)
NiO	0.38(0.01)	0.38(0.02)	0.27	0.010	0.39(0.02)	0.37(0.09)	0.41(0.02)	0.40(0.03)	0.05(0.03)
Total	99.95(0.15)	100.43(0.57)	99.77	100.25	100.09(0.6)	100.28(0.61)	100.01(0.35)	100.54(0.61)	99.98(0.29)
Fo	90.2	90.7	90.5	85.5	91.1	91.1	90.5	90.6	99.0
Abs	109(12)	105(22)	200(50)	658(75)	667(180)	652(270)	647(250)	555(240)	1167(145)
H_2O^1	21(2)	20(4)	38(9)	124(14)	125(34)	123(47)	121(47)	104(45)	219(27)
H_2O^2	8(1)	8(2)	14(3)	47(5)	34(9)	39(15)	36(14)	29(13)	103(13)
H_2O^3	10(1)	11(2)	20(5)	70(8)	45(12)	55(21)	51(20)	41(18)	151(19)

Abs = total OH absorption ($A^{E||x}+A^{E||y}+A^{E||z}$). Hydroxyl contents estimated using [1]Bell et al. (2003), [2]Paterson (1982), [3]Libowitzky and Rossman (1997).

(from 1100 to 1300 °C) than by increasing the duration of a relatively low temperature experiment (*i.e.* 1100 °C) by 100 h.

Polarised infrared absorbance spectra were collected from the cores of annealed olivine from SC1, SC2 and SC3 and from the Fe-rich overgrowths in SC3 (see the bottom three panels of Fig. 3). SC1 and SC2 were conducted at identical P, T and fO_2 but for 144 and 4 h respectively. Olivine from both these experiments contains identical hydroxyl species and dissolved water concentrations (Fig. 3; Table 3). Spectra collected through the cores of olivine from SC1, SC2 and SC3 show that, at the spatial resolution afforded by the infrared microscope (~100 μm), hydroxyl species dissolved in olivine crystals quenched from annealing experiments conducted at 1100 or 1300 °C, are identical (Fig. 3). Hydroxyl defects measured in the cores of all San Carlos olivine crystals annealed under low fO_2 conditions (SC1, SC2 and SC3) contain hydroxyl absorptions at 3612, 3575 and 3525 cm^{-1}.

Polarised spectra were collected on both generations of olivine from SC3 (*i.e.* 'normal' and 'Fe-enriched' compositions (Table 3)). Crystals that were re-equilibrated at low fO_2, but which retained the major element composition of the starting crystals, show a relatively weak shoulder centred at approximately 3598 cm^{-1}. This shoulder is not evident on spectra collected from the Fe-rich overgrowths, but these samples do show a pronounced absorption centred at 3593 cm^{-1} (Fig. 2). No olivine crystals re-equilibrated or grown under low fO_2 conditions contain hydroxyl defects with vibrational energies below 3400 cm^{-1} (low frequency absorptions).

Bell et al. (2003) used olivines with similar OH spectral characteristics to those recovered from our low

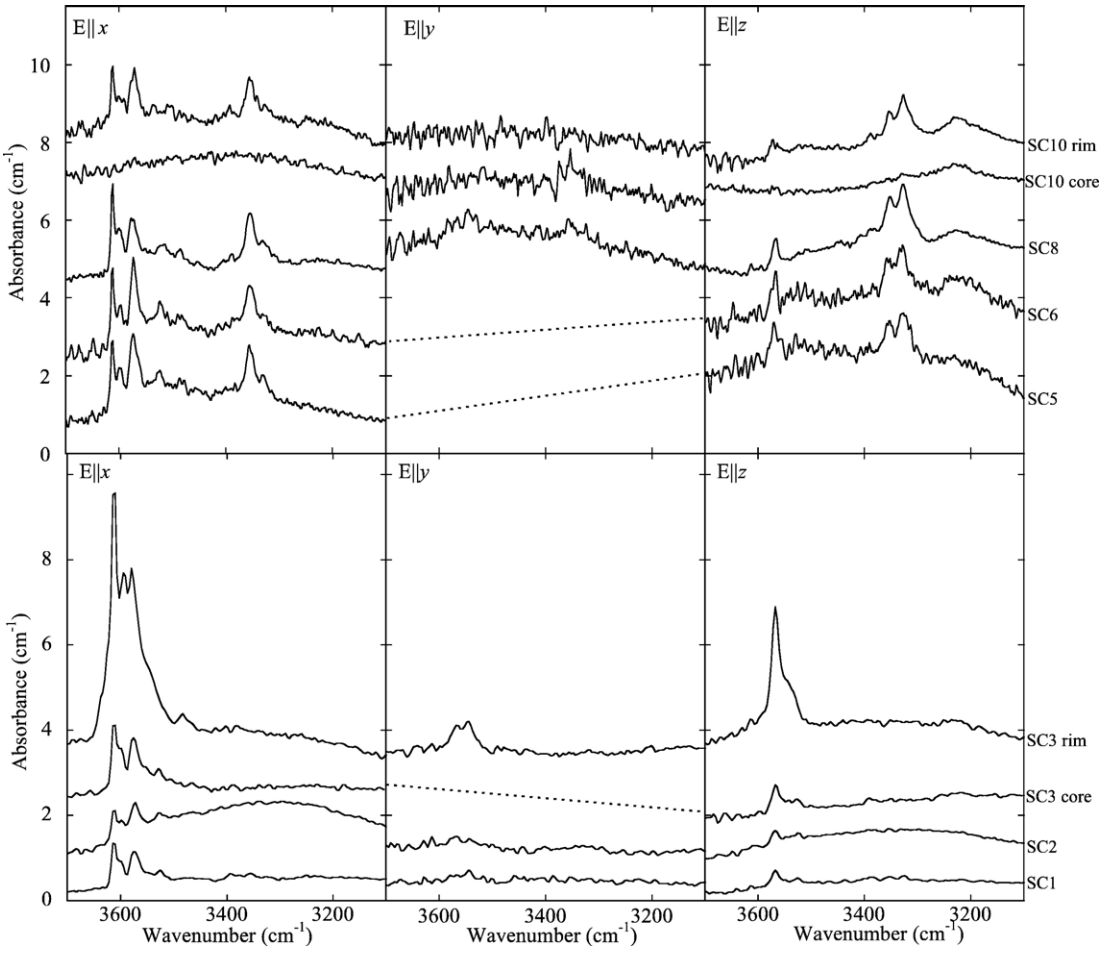

Fig. 3. Polarised infrared absorbance spectra collected on double polished sections of oriented olivine crystals recovered from each experiment described here. Spectra illustrated on the lower three panels were collected on crystals annealed or synthesised at fO_2 conditions controlled by the reaction Fe:FeO. Spectra in the upper three panels were measured on samples annealed at fO_2 imposed by the reactions Re:ReO_2 (SC5) or Ni:NiO (SC6, SC8, and SC10).

fO_2 experiments (*i.e.* only high frequency peaks) to derive a mineral-specific absorption coefficient. Using this, olivine from SC1 and SC2 both contain a similar amount of water; approximately 20 ppm H_2O (Table 3). Olivine from the core of SC3, which was annealed at 2.0 GPa and 1300 °C, contains almost twice that amount (38 ppm). The water contents of the Fe-rich secondary olivine overgrowths are several times higher than in the annealed olivine (approximately 124 ppm H_2O). Water contents derived using more general, wavenumber-dependent, calibrations (Paterson, 1982; Libowitzky and Rossman, 1997) are also provided on Table 3. These calibrations indicate that approximately 10 ppm H_2O is dissolved in olivine from SC1 and SC2 — approximately half of that calculated when the mineral-specific calibration is applied.

3.2.2. 'Higher' fO_2 experiments

The major element compositions of olivines from the relatively high fO_2 experiments (SC5, SC6 and SC10) were identical to those of the starting crystals. Most olivine recovered from these experiments had developed thin (several tens of microns) Ni-rich overgrowths during re-equilibration. Unfortunately, these were all too narrow to analyse using the infrared microscope. Experiment SC15b was conducted at 2 GPa, 1300 °C and run for 68 h without a foil oxygen buffer. Although olivine grains recovered from SC15b were morphologically similar to the starting crystals, electron microprobe analyses showed that they contain significantly less, FeO, CaO, NiO and MnO than the starting crystals. This compositional change is most likely due to high temperature diffusive re-equilibration (dilution) with the synthetic Fe-free talc:brucite matrix material in the absence of any Fe or Ni foil and/or loss of Fe to the Pt capsule during the experiment.

The top three panels of Fig. 3 show OH absorbance spectra of olivine from the higher fO_2 experiments. These samples were annealed using Ni (SC6, SC8 and SC10) or Re foil oxygen buffers (SC5), or at the relatively oxidising intrinsic fO_2 of the high-pressure assembly (SC15b). Olivine crystals from SC8803B and cubes of the large San Carlos crystal (SC cube) were used in different 'higher fO_2' annealing experiments (Table 2). Hydroxyl defect species dissolved in olivine from all higher fO_2 experiments are broadly analogous (Fig. 3). Hydroxyl concentrations dissolved in all olivine crystals recovered from experiments conducted for greater than 1 h are homogeneous. Olivine from SC5, SC6, SC8 and SC10 contain high-frequency OH aborptions at 3612, 3595, 3578, 3575 and 3525 cm^{-1}. Most of the defect species with vibrational energies between 3600–3400 cm^{-1} that are dissolved in olivine from the high fO_2 experiments are similar to those described in samples recovered from low fO_2 experiments. However, olivines from all of the higher fO_2 experiments also contain defect species which generate low-frequency absorptions at 3355, 3325, 3307 and 3160 cm^{-1} (Fig. 3). Hydroxyl defect speciation in crystals from SC15b differs slightly to others also annealed at higher fO_2. The low-Fe olivine from SC15b contains high frequency OH absorptions at **3623**, 3612, **3590**, 3578, **3570**, and low frequency peaks at **3450**, 3355 and 3325 cm^{-1} (those in bold are significantly different from the Fe-rich olivines).

Calculating the amount of water dissolved in olivine recovered from the higher fO_2 experiments is complicated by the fact that hydrous species dissolved in these crystals differ to those in samples used to calibrate the mineral-specific absorption coefficient (Bell et al., 2003) (*i.e.* they contain both high and low frequency absorptions). We, therefore, calculated water contents for these samples using the mineral-specific calibration (Bell et al., 2003) and two additional methods (Paterson, 1982; Libowitzky and Rossman, 1997). These latter calibrations yield wavenumber-dependent absorption coefficients and so provide an internally consistent method of quantifying hydroxyl in olivine from both the low and higher fO_2 experiments. Using Libowitzky and Rossman (1997), olivines annealed at 2.0 GPa and 1100 °C and under a high fO_2 regime (SC5, SC6 and SC8) contain approximately 45–55 ppm H_2O. This is marginally greater than the amount of water calculated from the same spectrum but using the alternative wavenumber-dependant calibration (Paterson, 1982) (34–39 ppm H_2O) and is less than half that obtained using Bell et al. (2003) (124 ppm H_2O). Using Libowitzky and Rossman (1997), the intensities of the OH absorbances present in Fe-poor olivine from SC15b correspond to a water content of approximately 150 ppm H_2O. Using the mineral-specific calibration of Bell et al. (2003), the same integrated OH absorbance corresponds to ~220 ppm H_2O.

Despite problems in precisely quantifying hydroxyl in the annealed olivines, our data illustrate that the total integrated OH absorbance for all crystals annealed under a relatively high fO_2 regime is up to four times greater than crystals annealed at identical P and T but under more reducing conditions (close to the Fe–FeO buffer, (Table 3)). The relative increase of fH_2 at low fO_2 conditions does not lead to a corresponding increase in dissolved hydroxyl concentrations and so it seems unlikely that fH_2 (as opposed to fH_2O) is the dominant factor controlling water solubility in olivine.

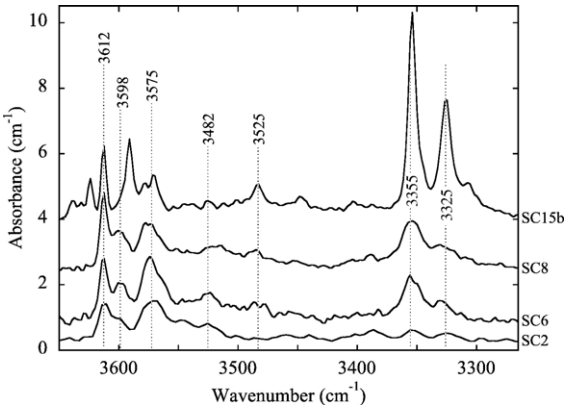

Fig. 4. OH absorbance spectra collected from olivine SC2, SC6, SC8 and SC15b. Spectra are the sum of absorbances measured where $E||x+E||y+E||z$ and have been selected to illustrate how fO_2 and major element chemistry effect hydroxyl speciation in olivine.

3.2.3. Rate of hydrogen incorporation and the creation of new hydrous defects

A cube of San Carlos olivine was annealed for at 2.0 GPa and 1100 °C (SC10) for 40 min in a Pt capsule lined with Ni foil. After the experiment, polished sections through the core of the cube were made parallel to the (100), (010) and (001) planes. Infrared spectra were then collected at increasing intervals perpendicular to the outer edge of the cube. The outermost termination of the cube, parallel to the (001) plane, contains hydrous defect species and concentrations that are identical to that in SC8 — a comparable experiment run at identical 2.0 GPa, 1100 °C and using a Ni foil oxygen buffer, but for 168 h. Hydroxyl speciation measured where $E||x$ at the edge of the sample parallel to the (010) plane is identical to similarly polarised spectra collected on crystals from SC8, but the concentrations of hydroxyl defects are less than those in olivine from the long duration run. No hydrous defects were identified at the outermost rim of the cube parallel to the (100) plane.

4. Discussion

4.1. Interpreting the significance of peak positions

We have shown that oxygen fugacity exerts a fundamental control on hydroxyl speciation and solubility in olivine. Total absorbance spectra ($A^{tot}=A^{E||x}+A^{E||y}+A^{E||z}$) from SC2, SC6, SC8 and SC15b are shown on Fig. 4. In experiments SC2 and SC6, single crystals of SC8803B olivine were re-equilibrated in the presence of enstatite and free fluid at 2.0 GPa and 1100 °C (Table 2). Oxygen fugacity in these experiments was controlled using Fe and Ni foil respectively. In SC8, a cube of San Carlos olivine was re-equilibrated at 2.0 GPa, 1100 °C and fO_2 was controlled by the reaction Ni–NiO. Each of the hydroxyl defect absorptions evident on spectra collected on olivine from SC2 (Fe buffered) are also found in Ni-buffered SC6 and SC8. However, spectra collected on olivine from all experiments conducted at higher fO_2 also contain hydroxyl absorptions at 3355, 3325, 3482 and 3230 cm^{-1} that are not found in any of the low fO_2 experiments (Fig. 3).

Hydroxyl defects between 3400 and 3300 cm^{-1} have been attributed to H at Si vacancies, singly charged oxygen interstitials (Bai and Kohlstedt, 1993; Libowitzky and Beran, 2004), magnesium vacancies (Kohlstedt et al.,1996; Kohlstedt and Mackwell, 1998; Matveev et al., 2001, 2005) or substitutional trivalent cations (Berry et al., 2005; Grant et al., 2006, 2007b). Absorbance spectra of olivine from SC2, SC5 and a number of synthetic forsterite samples (Lemaire et al., 2004; Grant et al., 2004, 2006, 2007b) are presented on Fig. 5. No OH absorptions between 3400–3300 cm^{-1} are found in spectra of pure (Fe-free) forsterite (Demouchy and Mackwell, 2003; Lemaire et al., 2004; Berry et al., 2005; Smyth et al., 2006; Grant et al., 2006) (It is worth noting here that the "pure" forsterite that contained low frequency OH absorptions presented by Zhao et al. (2004) contains several hundred ppm Fe (Table 1, Zhao et al., 2004). Aluminium-bearing forsterite crystals that were synthesised from a hydrous silicate melt contain Al^{3+}-related hydroxyl defects with vibrational energies of 3346 and 3322 cm^{-1} (Grant et al., 2006, 2007b) (Fig. 5). Berry et al. (2005) noted that OH absorptions at 3355 and 3325 cm^{-1} were only found in Fe-bearing synthetic

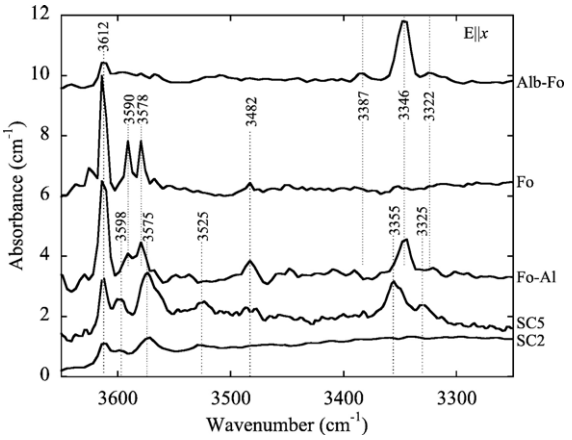

Fig. 5. OH absorbance spectra collected from a number of different olivine crystals. All spectra are polarised $E||x$ only. SC2 and SC5 are those described in this study. Fo–Al is forsterite, synthesised adjacent to trace Al-bearing enstatite (Matveev et al., 2001). Fo is pure forsterite (Lemaire et al., 2004). Alb–Fo is an Al-bearing forsterite crystal synthesised in the system Alb–Fo–H_2O (Grant et al., 2007b).

olivine and assigned these to hydroxyl groups associated with Fe^{3+} defects. Subsequent study has, however, shown that Cr^{3+}-related hydroxyl defects also generate absorptions at similar stretching frequencies (Berry et al., in press). Stretching energies of Al^{3+}-related OH species differ to Fe^{3+}-related OH groups (absorptions at 3346 and 3322 cm^{-1} for Al^{3+} *versus* 3350 and 3325 cm^{-1} for Fe^{3+}) because ionic radii of Al^{3+} and Fe^{3+} are significantly different. However, because the radii of Fe^{3+} and Cr^{3+} are more similar, the distinction between Fe^{3+} and Cr^{3+}-related hydroxyl defects is less obvious (Berry et al., in press).

Several lines of evidence, therefore, indicate that hydroxyl absorptions in olivine with vibrational energies between 3400–3300 cm^{-1} are attributable to protons incorporated in association with trivalent cations. The development of OH absorptions at 3355 and 3325 cm^{-1} in olivine crystals annealed at high fO_2 indicates that these defects are most likely associated with species that change valence across the range of oxygen fugacities that we have studied here. Theoretical calculations indicate that Fe^{3+} as both ($Fe^{\cdot}_{Me}$ on octahedral sites) and (Fe'_{Si} on tetrahedral sites) increases as a function of fO_2 (Stocker, 1978; Nakamura and Schmalzried, 1983; Hirsch and Shankland, 1993; Tsai and Dieckmann, 2002) and, as a result, we suggest that the most obvious candidate responsible for low energy OH peaks is Fe^{3+}.

One previous experimental study, conducted at high fO_2 (buffered by the reaction Re–ReO_2) and variable silica activity ($aSiO_2$), concluded that OH absorptions centred at 3355 and 3325 cm^{-1} in Fe-bearing olivine only developed at higher $aSiO_2$ and, as a result, were associated with metal vacancies (Fe or Mg) (Matveev et al., 2001). Similar conclusions, but for different low frequency absorptions, were drawn by Lemaire et al. (2004) for Fe-free (forsterite) olivines. However, these experimental observations have proven difficult to adequately explain because they contradict an earlier study (where the effect of $aSiO_2$ on hydroxyl speciation in olivine was found to negligible Bai and Kohlstedt, 1993) and have proven difficult to reproduce in subsequent studies (Mosenfelder et al., 2006a, 2006b).

4.2. Mechanisms and point defects

We now apply defect chemistry to interpret the mechanisms responsible for the incorporation of Fe^{3+}-related hydroxyl in olivine and show that observations from apparently contradictory studies (Bai and Kohlstedt, 1993; Matveev et al., 2001; Zhao et al., 2004; Berry et al., 2005; Mosenfelder et al., 2006b and the data presented here) can be satisfactorily reconciled.

Reaction between olivine and oxygen at elevated temperatures leads to the development of point defects in the crystal. Under oxidising conditions, excess oxygen is incorporated into the crystal structure and a number of different point defects must be contemporaneously created to retain charge balance. The primary mechanism of maintaining thermodynamic equilibrium during the incorporation of additional oxygen into olivine is through the creation of $Fe^{\cdot}_{Me}$ and/or Fe'_{Si} defects (Nakamura and Schmalzried, 1983; Tsai and Dieckmann, 2002). Following Nakamura and Schmalzried (1983) this process can be described using Kröger–Vink notation by:

$$2O_2(g) + Si^{x}_{Si} + 10Fe^{x}_{Me} = Fe_2SiO_4 + 3V''_{Me} + Fe'_{Si} + 7Fe^{\cdot}_{Me} \quad (1)$$

where Si^{x}_{Si} is a normally charged Si at a tetrahedral site, Fe^{x}_{Me} and V''_{Me} correspond to a divalent Fe cation and a metal vacancy on an octahedral site, respectively. Fe'_{Si} is an Fe^{3+} cation on a tetrahedral site and Fe_{Me}. is a trivalent Fe cation on an octahedral site. Following Eq. (1), the oxidation of olivine increases the concentrations of Fe^{3+} species at both tetrahedral and octahedral sites. Relatively high $aSiO_2$ suppresses Fe^{3+} substitution at tetrahedral sites and leads to vacancy formation at octahedral sites, as can be seen from:

$$2Fe^{x}_{Me} + Fe'_{Si} + 2SiO_2 = Si^{x}_{Si} + Fe_2SiO_4 + Fe^{\cdot}_{Me} + V''_{Me} \quad (2)$$

The results of this, and earlier experimental studies (Matveev et al., 2001), show that hydroxyl defects with vibrational energies at 3355 and 3325 cm^{-1} are found in olivine crystals re-equilibrated at relatively high $aSiO_2$. Therefore, in the following we assume that $Fe^{\cdot}_{Mg}$ is the dominant Fe^{3+} species dissolved in ferromagnesian olivine at the experimental conditions under which we observe the development of hydroxyl defects at 3355 and 3325 cm^{-1} (relatively high fO_2 and $aSiO_2$).

The overall reaction for the formation of $Fe^{\cdot}_{Mg}$ defects in olivine crystals from our higher fO_2 experiments can be described by:

$$3Fe^{x}_{Me} + \frac{1}{2}SiO_2 + \frac{1}{2}O_2 = 2Fe^{\cdot}_{Me} + V''_{Me} + \frac{1}{2}Fe_2SiO_4. \quad (3)$$

Eq. (3) highlights the critical importance of $aSiO_2$ and fO_2 in controlling the incorporation of $Fe^{\cdot}_{Me}$ into olivine because both high $aSiO_2$ and fO_2 are essential to stabilise $Fe^{\cdot}_{Me}$ defects. Thus, re-equilibrating olivine in experiments characterised by low $aSiO_2$ but high fO_2 (Matveev et al., 2001, 2005), relatively low fO_2 and

high $aSiO_2$ (as in this study) or low fO_2 and $aSiO_2$ (Bai and Kohlstedt, 1993) will all have the same negative effect on the concentration of $Fe^{\cdot}_{Me}$ defects. Therefore, if as suggested above, OH absorptions at 3355 and 3325 cm^{-1} are attributed to Fe^{3+}-related hydroxyl species, the experimental results of Matveev et al (2001, 2005), Bai and Kohlstedt (1993) and this study, are entirely consistent. Further studies into the relative fO_2 and $aSiO_2$ ranges under which Fe^{3+}-related hydroxyl defects develop in olivine, and the relative stability of these species under different thermodynamic environments, could form the basis of a tool with which to measure the relative $aSiO_2$ and fO_2 of host melts.

Although our results highlight a clear relationship between high fO_2 and $aSiO_2$ in the development of Fe^{3+}-related hydroxyl defects in mantle olivine, it should be noted that many previous studies (Bai and Kohlstedt, 1993; Matveev et al., 2005 and here) were conducted at 2.0 GPa or lower. The effect of pressure on the formation of Fe^{3+} point defects in olivine is unknown, although samples recovered from annealing experiments conducted at pressures in excess of 2.5 GPa and at relatively high fO_2 do not contain OH peaks at 3355 and 3325 cm^{-1} (Kohlstedt et al., 1996; Mosenfelder et al., 2006b). Further studies at high pressure are essential to help understand these important inconsistencies.

Hydroxyl defect absorptions at 3230 and 3160 cm^{-1} have been observed in enstatite-buffered olivines synthesised at oxidising or unbuffered (but likely oxidising) conditions (Lemaire et al., 2004; Berry et al., 2005; Grant et al., 2006, 2007b) and have been attributed to Mg vacancies charged balanced by hydrogen (Lemaire et al., 2004; Berry et al., 2005; Grant et al., 2006, 2007b)or paired Mg vacancies (Keppler and Bolfan-Casanova, 2006). Absorptions at 3230 and 3160 cm^{-1} are absent, or very small, in the Fe–FeO buffered samples from the present study (Fig. 3). This observation supports the suggestion that they are Mg vacancy-related defects because the concentration of these increases with oxygen fugacity (Stocker, 1978).

4.3. Dynamics of OH defect incorporation

At time scales relevant to the current study, hydration of iron-bearing olivine can occur *via* two processes (Kohlstedt and Mackwell, 1998; Ingrin and Blanchard, 2006). The first, and fastest, is the migration of hydrogen ions (H), a process charge compensated by a counter diffusion of charged electron holes ($h^{\cdot}$). H–$h^{\cdot}$ exchange kinetics at 1100 °C suggest that the hydroxyl contents of SC10 (approximately 2 mm in diameter) re-equilibrate under an imposed fH_2O regime in several seconds (Ingrin and Blanchard, 2006). However, the number of protons incorporated into the crystal structure and the OH defect speciation after H–$h^{\cdot}$ exchange is ultimately controlled by the concentrations of pre-existing crystal defects (*e.g.* V''_{Me} Kohlstedt and Mackwell, 1998; Ingrin and Grant, 2006) and/or impurity element substitutions (Ti and Fe^{3+} Berry et al., 2005; Al^{3+} Grant et al., 2006, 2007b). Although olivine from experiment SC2 (which was annealed at 2.0 GPa, 1100 °C and using a Fe foil oxygen buffer) does not contain hydroxyl defects with vibrational energies at 3325 and 3355 cm^{-1}, olivine from SC6 (which was annealed at identical P and T but at an fO_2 controlled by the reaction Ni:NiO), does. Thus, the development of OH absorptions at 3355 and 3325 cm^{-1} during annealing cannot be satisfactorily explained by H–$h^{\cdot}$ re-equilibration. Instead, at the time-scales of our experiments, the development of new hydroxyl defects indicates that new intrinsic hydrated point defects form at high fO_2. At 1100 °C, and for run durations of between 0.5 and 168 h, point defect formation in olivine is controlled by vacancy diffusion (D^{V}_{Me}) (Kohlstedt and Mackwell, 1998; Demouchy and Mackwell, 2006; Ingrin and Grant, 2006). Self-diffusion of metal vacancies is approximately two orders of magnitude slower than H–$h^{\cdot}$ exchange (Kohlstedt and Mackwell, 1998; Demouchy and Mackwell, 2006; Ingrin and Grant, 2006). The rate of metal vacancy re-equilibration by diffusion is consistent with the results of our relatively short-duration annealing experiment (SC10) and enforces our suggestion that hydroxyl species responsible for absorptions at 3355 and 3325 cm^{-1} in olivine are associated with Fe^{3+} defects. Furthermore, calculations using experimentally determined diffusion coefficients (Kohlstedt and Mackwell, 1998; Demouchy and Mackwell, 2006; Ingrin and Grant, 2006) indicate that point defect equilibrium should have been reached in all of our experiments except SC10.

Hydroxyl defects with vibrational energies of 3355 and 3325 cm^{-1} therefore develop in response to a relative increase in experimental fO_2 through a process of vacancy diffusion and hydration. Additional evidence to support this interpretation, and to illustrate the importance of metal vacancies in the development of OH peaks at 3325 and 3355 cm^{-1}, is found in SC10. This relatively short-duration experiment (30 min) shows that the incorporation of hydroxyl defects is greatest parallel to (001). Experimental studies have shown that H–$h^{\cdot}$ exchange is fastest along (100) or (010) whereas D^{V}_{Me} is greatest parallel to (001) (Kohlstedt and Mackwell, 1998; Ingrin and Blanchard, 2006).

4.4. Water solubility in mantle olivine

The maximum amount of hydroxyl that we have measured in Fo_{90} olivine recovered from water-saturated annealing experiments we describe here (Table 3) is lower than the current solubility laws suggest should be present in crystals re-equilibrated at the experimental P–T conditions used (Kohlstedt et al., 1996; Mosenfelder et al., 2006b). The reasons for this discrepancy remain uncertain although they perhaps highlight the necessity of careful experimental setup before water solubility in olivine can be accurately constrained. Previous investigations were conducted in smaller capsules than we have used here (1.6 to 2.0 mm diameter Kohlstedt et al., 1996; Mosenfelder et al., 2006b). This means that the relative volumes of talc: brucite buffer material and metal foil in the capsule will also differ. If these differences are large, the bulk chemical composition of different experiments may be sufficient to alter the intensive thermodynamic properties of the system. For example, the growth of olivine containing a Ni_2SiO_4 component around crystals (Kohlstedt et al., 1996) implies oxidation of a relatively large mass of Ni metal to NiO. Growth of such Ni_2SiO_4-rich olivine also consumes SiO_2 from the talc:brucite buffer. This could reduce $aSiO_2$ of the aqueous fluid if, for example, insufficient enstatite is in contact with the fluid to maintain SiO_2 buffering, and could increase water solubility in olivine (c.f. water concentrations of olivine from MgO-buffered and En-buffered experiments reported elsewhere Matveev et al., 2001).

Accurately quantifying hydroxyl in olivine remains extremely difficult and may also result in inter-study discrepancies. We found that hydroxyl in olivine from our high fO_2 experiments was more difficult to accurately quantify than that in samples from low fO_2 experiments. This was mostly because hydroxyl absorptions on spectra collected on olivine from the higher fO_2 experiments were superimposed upon undulating backgrounds, but also because there is no mineral-specific calibration for samples in which low frequency absorptions contribute significantly to the overall hydroxyl budget. Despite these problems, however, the relative concentrations of absorbing species between 3650–3450 cm^{-1} that are dissolved in different samples can be readily estimated by applying the mineral-specific calibration (Bell et al., 2003) to the integrated OH absorbance in this region of the spectrum alone. Doing so demonstrates that hydroxyl defects responsible for absorptions at high frequencies (3650–3450 cm^{-1}) in olivine from low fO_2 (SC2) and higher fO_2 (SC6) experiments amount to approximately 20 (±5) and 35 (±5) ppm H_2O respectively. Regardless of potential inaccuracies in quantifying hydroxyl in the samples, these measurements tell us that the relative number of absorbing species between 3650 and 3450 cm^{-1} in samples annealed at higher fO_2 is greater than those in samples annealed at low fO_2. The true difference in total dissolved water contents must, however, be greater than this because samples annealed at higher fO_2 contain additional bands at low frequencies between 3400–3000 which are not quantified using this method. Relative amounts of water dissolved in samples annealed under different fO_2 regimes are therefore perhaps best estimated and compared using a wavenumber-dependent calibration. As can be seen from Table 3, when samples from experiments conducted at identical P–T and run durations are considered, those from high fO_2 experiments contain approximately five times more hydroxyl than samples annealed at low fO_2.

5. Geological implications

Oxygen fugacity is an important parameter in many geochemical processes within the Earth. We have demonstrated the importance of fO_2 in determining hydroxyl speciation and concentrations in experimentally annealed olivine. Olivine crystals annealed under relatively more oxidising conditions (NNO) contain at least three times as much water as those annealed using a an Fe foil oxygen buffer (IW). These observations are perhaps unsurprising as fO_2 fundamentally controls point defect concentrations in olivine (Stocker, 1978; Stocker and Smyth, 1978; Nakamura and Schmalzried, 1983; Tsai and Dieckmann, 2002). Current water solubility laws were constructed following a series of water-saturated hydrothermal annealing experiments at 1100 °C and where fO_2 was buffered by the reaction Ni: NiO or the high-pressure sample assembly (Kohlstedt et al., 1996; Mosenfelder et al., 2006b). Several studies have now documented the ambient fO_2 of the primitive mantle of the Earth and have demonstrated that fO_2 of the lithosphere decreases with depth (McCammon et al., 2001; Woodland and Koch, 2003; McCammon and Kopylova, 2004). At shallow depths, where spinel peridotite is stable, log fO_2 values of approximately QFM-1 are obtained (Woodland and Koch, 2003). However, at approximately 200 km depth log fO_2 may be less than QFM-4 (McCammon et al., 2001; Woodland and Koch, 2003). Our data suggest that extrapolating a value for the solubility of water in olivine from experiments conducted at approximately QFM could overestimate the amount of water dissolved in olivine at depth in the Earth by at least a factor of two. This would have

significant implications for the storage of water in the upper mantle of the Earth and impact greatly on melting, phase relations and rheology.

6. Conclusions

In this study we have shown that, at a pressure of 2.0 GPa, the intensities of OH peaks at 3355 and 3325 cm^{-1} increase as a function of fO_2. This implies association with the conversion of Fe^{2+} to Fe^{3+}, a process requiring additional charge balance, probably by V''_{Me} formation. OH peaks at similar vibrational energies are observed in forsterite crystals containing trace Al^{3+}, thus reinforcing the connection of OH defect species between 3400–3300 cm^{-1} to trivalent cation substitutions. OH absorptions at 3325 and 3355 cm^{-1} are relatively common in mantle-derived olivine (Miller et al., 1987; Bell and Rossman, 1992; Bell et al., 2004; Matsyuk and Langer, 2004; Berry et al., 2005; Matveev et al., 2005; Mosenfelder et al., 2006a; Demouchy et al., 2006; Peslier and Luhr, 2006; Grant et al., 2007a). Furthermore, olivine from the same geographic locality may show highly variable OH defect populations (Grant et al., 2007a) with variable proportions of low and high frequency peaks. If the point defect population of mantle-derived olivine were controlled by the melt in which the xenoliths were included then, OH absorptions related to oxidation/reduction of iron, should simply reflect the fO_2 of the magma. At Kilbourne Hole, this is clearly not the case (Grant et al., 2007a) and implies that the OH stretching signature was inherited directly from the mantle.

The solubility of water in hydrothermally annealed olivine is less than would be calculated for the appropriate *P–T* conditions using current models (Kohlstedt et al., 1996; Mosenfelder et al., 2006b). Furthermore, our study shows that fO_2 significantly influences the amount of water dissolved in olivine crystals annealed under otherwise identical conditions. These results indicate that the solubility of water in olivine from the garnet peridotite field of the lithospheric upper mantle may currently be overestimated by more than a factor of two.

Acknowledgements

The support of the National Environmental Research Council (NERC) and the Australian Research Council (ARC) are gratefully acknowledged. This study used instrumentation and geochemical laboratories funded by ARC LIEF and DEST Systemic Infrastructure Grants, Macquarie University and industry. Thanks to Jed Mosenfelder and an anonymous reviewer for their helpful comments, and to Rick Carlson for his editorial handling. KJG was supported by NERC grant NER/A/S/2002/00871. BJW was supported by NERC grant NE/B502936/1. This is contribution no. 478 from the ARC GEMOC National Key Centre (www.es.mq.edu.au/GEMOC/).

References

Bai, Q., Kohlstedt, D.L., 1992. Substantial hydrogen solubility in olivine and implications for water storage in the mantle. Nature 375, 672–674.

Bai, Q., Kohlstedt, D.L., 1993. Effects of chemical environment on the solubility and incorporation mechanism for hydrogen in olivine. Phys. Chem. Miner. 19, 460–471.

Bell, D.R., Rossman, G.R., 1992. Water in the Earth's upper mantle, the role of nominally anhydrous minerals. Science 255, 1391–1397.

Bell, D.R., Rossman, G.R., Maldener, J., Endisch, D., Rauch, F., 2003. Hydroxide in olivine: a quantitative determination of the absolute amount and calibration of the IR spectrum. J. Geophys. Res 108, 2105.

Bell, D.R., Rossman, G.R., Moore, R.O., 2004. Abundance and partitioning of OH in a high pressure magmatic system: megacrysts from the Monastery Kimberlite, South Africa. J. Petrol. 45, 1539–1564.

Berry, A.J., Hermann, J., O'Neill, H.S.C., Foran, G.J., 2005. Fingerprinting the water site in mantle olivine. Geology 33, 869–872.

Berry, A., O'Neill, H.S.C., Hermann, J., Scott, D.R., in press. The infrared signature of water associated with trivalent cations in olivine, Earth Planet. Sci. Lett. doi:10.1016/j.epsl.2007.02.021.

Brooker, R.A., Holloway, J.R., Hervig, R.L., 1998. Reduction in piston cylinder experiments: the detection of carbon infiltration into platinum capsules. Am. Mineral. 83, 985–994.

Demouchy, S., Mackwell, S.J., 2003. Water diffusion in synthetic iron-free forsterite. Phys. Chem. Miner. 30, 486–494.

Demouchy, S., Mackwell, S.J., 2006. Mechanisms of hydrogen incorporation and diffusion in iron-bearing olivine. Phys. Chem. Miner. 33, 347–355.

Demouchy, S., Jacobsen, S.D., Gaillard, F., Stern, C.R., 2006. Rapid magma ascent recorded by water diffusion profiles in mantle olivine. Geology 34, 429–432.

Grant, K.J., Kohn, S.C., Brooker, R.A., 2004. Hydrogen partitioning between synthetic olivine, orthopyroxene and melt. Geochim. Cosmochim. Acta 68, A34.

Grant, K.J., Kohn, S.C., Brooker, R.A., 2006. Solubility and partitioning of water in synthetic forsterite and enstatite in the system MgO–SiO_2–H_2O±H_2O. Contrib. Mineral. Petrol. 151, 651–664.

Grant, K.J., Ingrin, J., Lorand, J.-P., Dumas, P., 2007a. Water partitioning between in mantle minerals from peridotite xenoliths. Contrib. Mineral. Petrol. 154, 15–34.

Grant, K.J., Kohn, S.C., Brooker, R.A., 2007b. The partitioning of water between olivine, orthopyroxene and melt in the system Albite–Forsterite–H_2O. Earth Planet. Sci. Lett. 260, 227–241.

Hirsch, L.M., Shankland, T.J., 1993. Quantitative olivine-defect chemical model: insights on electrical conduction, diffusion, and the role of Fe content. Geophys. J. Int.

Ingrin, J., Blanchard, M., 2006. Diffusion of hydrogen in mantle minerals. In: Keppler, H., Smyth, D.M. (Eds.), Water in Nominally Anhydrous Minerals 62. Mineralogical Society of America, Washington D.C., pp. 291–320.

Ingrin, J., Grant, K.J., 2006. H profiles in mantle xenoliths: constraints from diffusion data. Geochim. Cosmochim. Acta 70, A277.

Keppler, H., Bolfan-Casanova, N., 2006. Thermodynamics of water solubility and partitioning. In: Keppler, H., Smyth, J.R. (Eds.), Water in Nominally Anhydrous Minerals, Reviews in Mineralogy 62. Mineralogical Society of America, Washington D.C., pp. 193–230.

Kohlstedt, D.L., Mackwell, S.J., 1998. Diffusion of hydrogen and intrinsic point defects in olivine. Z. Phys. Chem. 207, 147–162.

Kohlstedt, D.L., Keppler, H., Rubie, D.C., 1996. Solubility of water in the α-phase, β-phase and γ-phase of $(Mg,Fe)_2SiO_4$. Contrib. Mineral. Petrol. 123, 345–357.

Lemaire, C., Kohn, S.C., Brooker, R.A., 2004. The effect of silica activity on the incorporation mechanisms of water in synthetic forsterite: a polarised infrared spectroscopic study. Contrib. Mineral. Petrol. 147, 48–57.

Libowitzky, E., Beran, A., 2004. IR spectroscopic characterisation of hydrous species in minerals. In: Beran, A., Libowitzky, E. (Eds.), Spectroscopic Methods in Mineralogy, EMU Notes in Mineralogy 6. European Mineralogical Union, Budapest, pp. 227–279.

Libowitzky, E., Rossman, G.R., 1997. An IR absorption calibration for water in minerals. Am. Mineral. 82, 1111–1115.

Matsyuk, S.S., Langer, K., 2004. Hydroxyl in olivines from mantle xenoliths in kimberlites of the Siberian Platform. Contrib. Mineral. Petrol. 147, 413–437.

Matveev, S., O'Neill, H.S.C., Ballhaus, C., Taylor, W.R., Green, D.H., 2001. Effect of silica activity on OH-IR spectra of olivine: implications for low-aSiO_2 mantle metasomatism. J. Petrol. 42, 721–729.

Matveev, S., Portnyagin, M., Ballhaus, C., Brooker, R.A., Geiger, C.A., 2005. FTIR spectrum of phenocryst olivine as an indicator of silica saturation in magmas. J. Petrol. 46, 603–614.

McCammon, C., Kopylova, M.G., 2004. A redox profile of the Slave mantle and oxygen fugacity control in the cratonic mantle. Contrib. Mineral. Petrol. 148, 55–68.

McCammon, C.A., Griffin, W.L., Shee, S.R., O'Neill, H.S.C., 2001. Oxidation during metasomatism in ultramafic xenoliths from the Wesselton kimberlite, South Africa: implications for the survival of diamond. Contrib. Mineral. Petrol. 141, 2870296.

McDade, P., Wood, B., Van Westrenen, B.W.R., Gudmundsson, G., Soulard, H., Najorka, J., Blundy, J., 2002. Pressure corrections for a selection of piston-cylinder assembles. Mineral. Mag. 66, 1021–1028.

Miller, G.H., Rossman, G.R., Harlow, G.E., 1987. The natural occurrence of hydroxide in olivine. Phys. Chem. Miner. 14, 461–472.

Mosenfelder, J.L., Sharp, T.G., Asimow, P.D., Rossman, G.R., 2006a. Hydrogen Incorporation in Natural Mantle Olivines, Water in the Mantle. American Geophysical Union, Washington.

Mosenfelder, J.L., Deligne, N.I., Asimow, P.D., Rossman, G.R., 2006b. Hydrogen incorporation in olivine from 2–12 GPa. Am. Mineral. 91, 285–294.

Nakamura, A., Schmalzried, H., 1983. On the non-stoichiometry and point defects of olivine. Phys. Chem. Miner. 10, 27–37.

O'Neill, H.S.C., 1988. Systems Fe–O and Cu–O: thermodynamic data for the equilibria of Fe–"FeO," Fe–Fe_3O_4, "FeO"–Fe_3O_4, Fe_3O_4–Fe_2O_3, Cu–Cu2O and Cu_2O–CuO from emf measurements. Am. Mineral. 73, 470–487.

O'Neill, H.S.C., Pownceby, M.I., 1993. Thermodynamic data from redox reactions at high-temperatures. 1. An experimental and theoretical assessment of the electrochemical method using stabilized zirconia electrolites, with revised values for the Fe–FeO, Co–CoO, Ni–NiO and Cu–Cu_2O oxygen buffers, and new data from the W–WO_2 buffer. Contrib. Mineral. Petrol. 114, 296–314.

Paterson, M.S., 1982. The determination of hydroxyl by infrared absorption in quartz, silicate glasses and similar materials. Bull. Minérallogie 105, 20–29.

Peslier, A.H., Luhr, J.F., 2006. Hydrogen loss from olivines in mantle xenoliths from Simcoe (USA) and Mexico: mafic alkalic magma ascent rates and water budget of the sub-continental lithosphere. Earth Planet. Sci. Lett. 242, 302–319.

Smyth, J.R., Frost, D.J., Nestola, F., Holl, C.M., Bromiley, G., 2006. Olivine hydration in the deep upper mantle: effects of temperature and silica activity. Geophys. Res. Lett. 33 doi:10.1029/2006GL026194.

Stocker, R.L., 1978. Influence of oxygen pressure on defect concentrations in olivine with a fixed cationic ratio. Phys. Earth Planet. Inter. 17, 118–129.

Stocker, R.L., Smyth, D.M., 1978. Effect of enstatite activity and oxygen partial pressure on the point-defect chemistry of olivine. Phys. Earth Planet. Inter. 16, 145–156.

Tsai, T.-L., Dieckmann, R., 2002. Variation in the oxygen content and point defects in olivines, $(Fe_xMg_{1-x})_2SiO_4$, $0.2 \le x \le 1.0$. Phys. Chem. Miner. 29, 680–694.

Wood, B.J., Virgo, D., 1989. Upper mantle oxidation state: ferric iron contents of lherzolite spinels by ^{57}Fe Mossbauer spectroscopy and resultant oxygen fugacites. Geochim. Cosmochim. Acta 53, 1277–1291.

Woodland, A.B., Koch, M., 2003. Variation in oxygen fugacity with depth in the upper mantle beneath the Kaapvaal craton, Southern Africa. Earth planet. Sci. Lett. 214, 295–310.

Zhao, Y.-H., Ginsberg, S.B., Kohlstedt, D.L., 2004. Solubility of hydrogen in olivine: dependence on temperature and iron content. Contrib. Mineral. Petrol. 23, 1–10.